A self-powered triboelectric negative ion generator in pipeline

Fangming Li [a],[1], Cuiwen Deng [a],[1], Minzheng Sun [a],[1], Xingfu Wan [a], Shuowen Sun [a], Weipeng Xu [a], Taili Du [a], Yongjiu Zou [a], Haichao Yuan [a], Xinxiang Pan [a],[b], Jianchun Mi [a],[c], Minyi Xu [a],[*]

[a] Dalian Key Lab of Marine Micro/Nano Energy and Self-powered Systems, Marine Engineering College, Dalian Maritime University, Dalian 116026, China
[b] School of Electronics and Information technology, Guangdong Ocean University, Zhanjiang 524088, China
[c] College of Engineering, Peking University, Beijing 100871, China

A B S T R A C T

Indoor air quality plays a critical role in maintaining human health and well-being. In this study, a novel self-powered and high-efficiency negative air ion (NAI) generator in pipeline is proposed for air purification in the ventilation system. The self-power is achieved by utilizing a novel device of wind energy triboelectric nanogenerator (WE-TENG) to efficiently harvest wind energy in the pipeline. The present WE-TENG of investigation can reach a high rotation speed of 1300 rpm at 5.5 m/s in the pipe with a pressure drop of 175 Pa. After the power management circuit, the self-powered NAI generator is capable to drive 21 carbon-fiber electrodes to generate NAIs, with a generation rate of 23.14 μC/s. The self-powered NAI generator efficiently generates a high volume of NAIs in the pipeline, harnessing the air-purifying properties of NAIs, thereby making a significant impact on the practical application of self-powered indoor air purification systems based on TENG.

1. Introduction

The quality of air is paramount to human health [1,2], and its improvement could save numerous lives [3]. As individuals spend the majority of their time indoors, indoor air quality has become a matter of significant concern [4–7]. However, the complexity of power supply and maintenance requirements for conventional air purification equipment poses significant challenges [8–10]. Since the advent of TENG [11], many solutions have been devised to purify indoor air using the high voltage (HV) electricity generated by TENG with positive results [12–17]. Especially, the employment of a motion-stimulated triboelectric negative air ion (NAI) generator has demonstrated the capability to produce up to 1×10^{13} NAIs and purify air efficiently [14]. Despite this, the limitations in the power generation capacity of TENG and the energy recovery strategy still hinder the practical implementation of TENG-based self-powered air purification systems.

Until now, the performance of rotary TENG has been greatly improved through various optimizations, including self-healing design [18], reducing triboelectric charge decay [19], structural design [20,21], material selection [22], and charge pumping strategy [23]. Especially, a polyester fur-reinforced rotary triboelectric nanogenerator (PFR-TENG) exhibits the advantages of low friction and high output

voltage, making it well-suited for wind energy harvesting [24]. Studies on the utilization of rotary TENGs for wind energy harvesting have been extensively conducted [21,24–31], resulting in the development of energy harvesting systems and self-powered sensing systems. In particular, the use of rotary TENG in ventilation systems offers the possibility of energy recycling and self-powered real-time monitoring [25]. In addition to powering the sensors, the energy collected from wind energy by TENGs has been applied in various fields such as oil-water separation [32], plant growth [24], and anti-fogging [33], which take full advantage of the HV output characteristics of TENGs. Moreover, with the HV characteristics of TENG, the TENG has also enabled the use of an electroaerodynamics thruster based on the ionic wind theory, demonstrating its ability to generate large amounts of NAIs [34]. With these capabilities, using the rotary TENG to harvest wind power in pipe and generate NAIs to purify the air presents a promising solution.

This paper reports an innovative lab-scale self-powered NAI generator in pipeline. The self-powered NAI generator leverages pipeline wind energy captured by a wind energy triboelectric nanogenerator (WE-TENG), which is comprised of two PFR-TENGs and blades. The HV electricity generated by the WE-TENG is regulated by a power management circuit (PMC) to an appropriate voltage and produces a large amount of NAIs. The WE-TENG exhibits a low start-up wind speed of 1.5

m/s, capable of rotating continuously at 50 rpm while achieving a high wind energy harvesting efficiency with the ability to reach up to 1300 rpm at a wind speed of 5.5 m/s. By connecting both ends of the WE-TENG in parallel, the short-circuit current is doubled than one end of the WE-TENG. This results in a short-circuit current of up to 150 μA and an open-circuit voltage of 5 kV at 1300 rpm. The WE-TENG is further equipped with a voltage doubler and generates a maximum direct current of 9 kV at 1300 rpm, which can drive 21 carbon-fiber electrodes to produce NAIs. When all of the above devices are placed in the pipeline, the self-powered NAI generator has a low pressure drop, with only 8 Pa at a wind speed of 1.5 m/s and rising to 175 Pa at 5.5 m/s. Through a series of experiments, the efficacy of the self-powered NAI generator in air purification is rigorously established. The performance of the self-powered NAI generator in the pipeline offers a robust foundation for the implementation of TENG-based air purification systems in practical applications.

2. Results and discussion

2.1. Working principle of the self-powered NAI generator

Fig. 1a shows the application scenario of the self-powered NAI generator placed in a pipeline, using wind energy to generate large amounts of NAIs. By adsorbing the dust in the air, NAIs allow the dust to
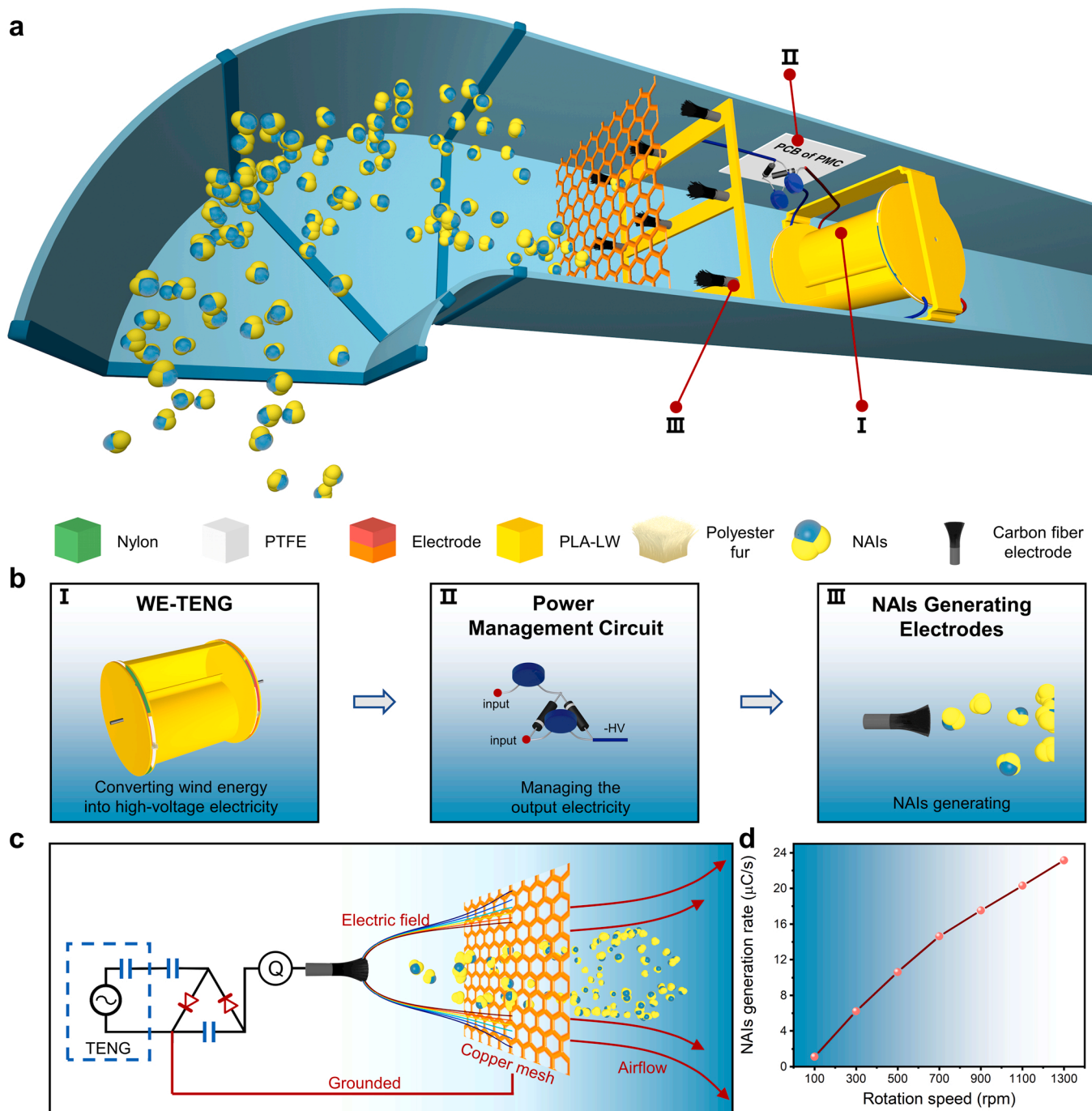

Fig. 1. Schematic illustrations of the self-powered NAI generator and the application scenario. (a) Application scenario diagram of the self-powered NAI generator in generating NAIs and purifying the air in a pipeline. (b) The system components of the self-powered NAI generator. (c) Schematic diagram of the grounding copper mesh to enhance the generation of NAIs. (d) The NAIs generation rate with 21 carbon fiber electrodes at different rotation speeds.

settle and thus purify the air. The self-powered NAI generator can be applied in the pipeline of the ventilation system, exhaust systems, etc. to achieve self-powered air purification.

The composition of the self-powered NAI generator is presented in Fig. 1b, which incorporates three essential elements, including the WE-TENG, the PMC, and an electrode array. The self-powered NAI generator collects wind energy in the pipeline by WE-TENG and converts it into HV electrical energy through triboelectric effect and electrostatic induction. A PMC adjusts the output of the WE-TENG to the optimal voltage for generating NAIs. Eventually, at the tip of the electrode, a strong electric field ionizes the air and generates a large amount of negative NAIs.

As shown in Fig. 1c, connecting the copper mesh to the ground can greatly enhance the electric field strength at the electrode tip, which is due to the increased potential gradient. The greater electric field strength enhances the generation rate of NAIs, which results in better performance of the self-powered NAI generator, compared to without grounded copper mesh. Since the copper mesh has large porosity, the majority of NAIs generated by the electrodes can pass through the mesh and disperse into the air. To measure the charge of the generated NAIs, a charge meter is connected in series between the PMC and the electrodes. When a charge meter is directly connected between an electrode and a copper mesh, the internal resistance of the meter is typically much smaller than the equivalent resistance of the air during NAIs generation. This can negatively impact the operation of the circuit. However, by connecting the charge meter between the PMC and the electrode, it can accurately record the amount of charge passing through the circuit while still allowing for the normal release of NAIs from the electrode.

Fig. 1d shows the generation rate of NAIs using 21 carbon-fiber electrodes at different rotation speeds. The self-powered NAI generator can generate 1.1 µC of NAIs per second at the rotation speed of 100 rpm. The generation rate of NAIs reaches the maximum of 23 µC/s at the rotation speed of 1300 rpm, corresponding to a wind speed of 5.5 m/s. Therefore, the self-powered NAI generator can efficiently and

self-powered generate NAIs and purify the air.

2.2. Structure and performance of WE-TENG

Fig. 2a & b show the cross-section and structure of the WE-TENG. The WE-TENG is composed of two blades, each with a cross-sectional geometry of two semicircles, featuring distinct radii of $R = 59.5$ mm and $r = 8.5$ mm. This design is found to allow for efficient collection of wind energy and minimization of pressure drop.

Two PFR-TENGs are integrating at both ends of the WE-TENG, achieving high integration and enabling efficient wind power generation in the pipeline. The material of the PFR-TENG is shown in Fig. 2c. Alternating arrangements of PTFE and nylon and three pairs of electrodes are incorporated to generate HV electricity, which is sufficient to meet the threshold voltage requirement (in general above 1 kV) for NAI generation [35–37]. As shown in Fig. 2d, the WE-TENG starts up and rotates continuously at 50 rpm at the wind speed of 1.5 m/s, reaching 1300 rpm at the wind speed of 5.5 m/s. Fig. 1e depicts the low pressure drop before and after the WE-TENG keeps low at different wind speeds, ensuring minimal impact on the normal operation of the ventilation system. Fig. 2f compares the rotation speed of the present WE-TENG with those of previous TENG-based wind harvesting devices [21, 26–31] fitted to the same wind speed of 5 m/s. This comparison clearly demonstrates that the WE-TENG can obtain a far higher rotational speed than other TENG-based wind turbines in the open area. The high speed and efficiency of the WE-TENG are dependent on its unique vertical axis blade design and the working environment in the pipeline. Based on the capacitive model of the TENG [38], the output current of the TENG can be expressed as:

$$I = A \frac{\mathrm{d}\delta}{\mathrm{d}t} \tag{1}$$

where A and δ represent effective contact area and surface charge den-
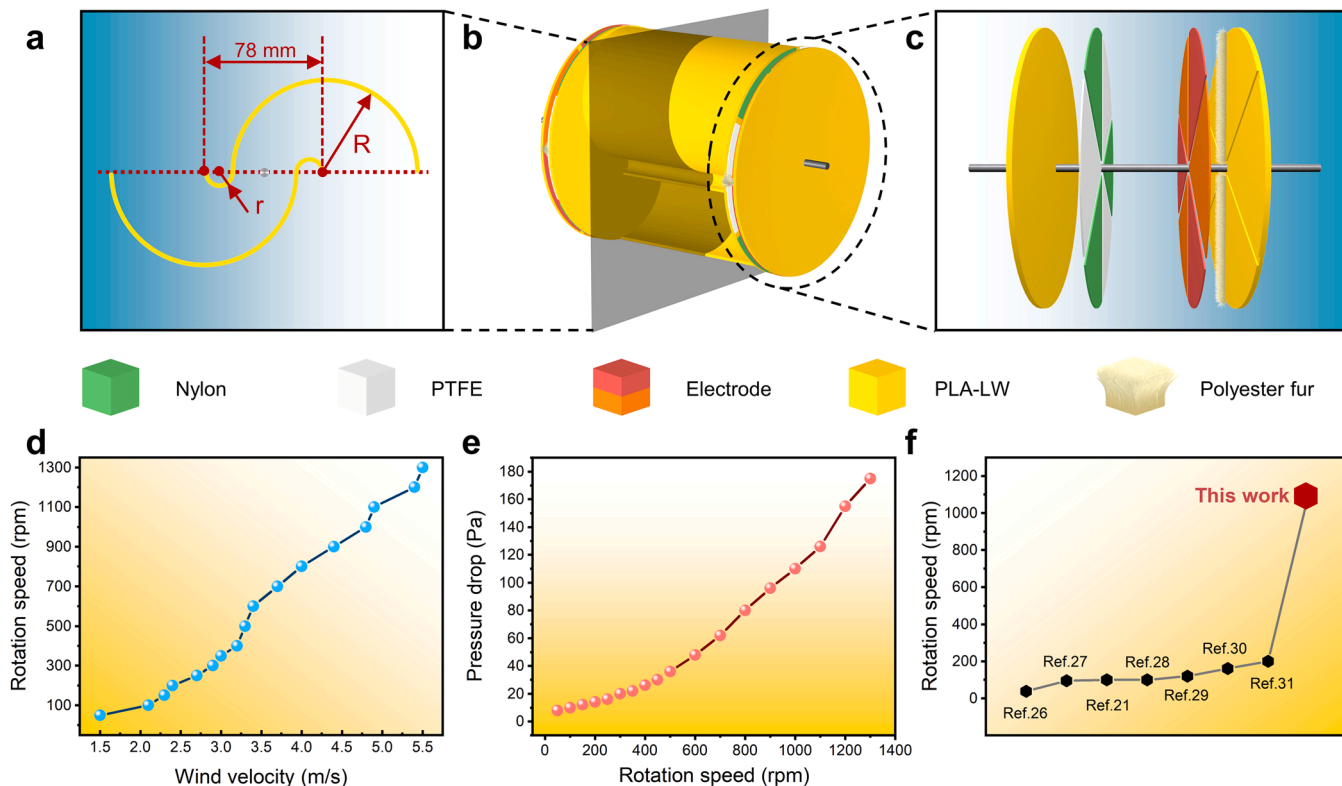

Fig. 2. Structure and working performance of the WE-TENG. (a) The cross-section, (b) the structural representation, and (c) the materials of the WE-TENG. (d) The rotation speed of WE-TENG versus the wind speed. (e) The pressure drop of self-powered NAI generator at different wind speeds. (f) Comparison between the present WE-TENG with previous TENG-based wind harvesting devices [21,26–31] on the rotation speeds fitted to a wind speed of 5 m/s.

sity respectively. When the triboelectric effect of TENG reaches saturation, the output voltage and δ remain constant, which means the high rotation speed of the WE-TENG enables it to obtain higher output current and better power generation performance. As shown in **supporting video 1**, the WE-TENG can easily light up a hundred 36 V-rated light emitting diodes (LEDs), which proves that the WE-TENG has enough power to generate NAIs.

Supplementary material related to this article can be found online at doi:10.1016/j.nanoen.2023.108459.

2.3. Electrical characteristics and power management of the WE-TENG

The working mechanism of the WE-TENG is shown in Fig. 3a. The WE-TENG utilizes three dielectric materials with different charge affinities, which are nylon, polyester fur, and PTFE. In this study, the use of two pieces of polyester fur is adopted to ensure power generation performance and reduce friction. The polyester fur exhibits an intermediate charge affinity between nylon and PTFE, acting as a charge pump and transmitting charge between alternating layers of nylon and PTFE. The fully charged nylon and PTFE induce a positive and negative electric field on electrodes, thereby amplifying the potential difference compared to the TENG which only uses two dielectric materials, resulting in a high voltage output.

In Figs. 3b & c and S1, the open-circuit voltage (V_{OC}), short-circuit current (I_{SC}), and short-circuit transferred charge (Q_{SC}) of one end of the WE-TENG are systematically characterized as a function of rotation speed (n). The results show that V_{OC} increases from 2 kV to the maximum of 6 kV as n increases from 50 rpm to 1100 rpm. After 1100 rpm the voltage is slightly reduced to 5.5 kV due to the excessive speed that leads to poor friction. Meanwhile, Q_{SC} remains constant, and I_{SC} increases with n, reaching $I_{SC} = 75$ μA at $n = 1300$ rpm.

In this study, a parallel connection is chosen to connect both ends of the WE-TENG. As illustrated in Figs. 3d and S2 & S3, I_{SC} and Q_{SC} are doubled after parallel connection, while V_{OC} remains the same. With the parallel connection, I_{SC} increases to 150 μA at $n = 1300$ rpm, ensuring sufficient capacity for powering four PMCs.

Fig. 4a shows the equivalent circuit diagrams of four PMCs. They are (PMC-I) the full wave rectifier circuits, (PMC-II) the Villard circuit using the internal capacitor of the TENG which is represented by C_{TENG}, (PMC-III) the Villard circuit, and (PMC-IV) the voltage doubler. The equivalent circuit diagram for measuring their output voltages is shown in Fig. S4, and corresponds to the output of the PMCs at a load of 1 GΩ.

Fig. 4b displays the stabilized output voltages of the four PMCs for $n = 700$ rpm. The PMC-I transforms the AC output of the WE-TENG into pulsed DC with equal amplitude. PMC-II and PMC-III increase the amplitude of the voltage while converting AC to pulsed DC. However, the small internal capacitor of the WE-TENG limits the ability of PMC-II to double the amplitude, while PMC-III is capable. The output voltage of PMC-IV is shown in Fig. S5, which reaches stability with a DC output of approximately 7 kV after charging 2 s. As shown in Fig. S6, the stable output of PMC-IV varies as n changes. As n increases, the output voltage of PMC-IV on the load of 1 GΩ increases from 1.5 kV to 9 kV.

2.4. Performance of self-powered NAI generator in generating NAIs

The NAIs generated by the self-powered NAI generator are produced on an electrode made of a unique material. Fig. 5a shows three different electrodes which are tungsten-alloy, needle, and carbon-fiber electrodes. Each electrode generates NAIs by connecting it to the negative HV end of the PMC. When the electrodes are connected to their circuits, thereby producing a strong electric field on the electrode tip that ionizes the air and results in the generation of NAIs.

In our experiment, the distance (L) between the electrode and the copper mesh needs to be greater than 2 cm to avoid a discharge arc. The electric field simulation has been performed using COMSOL to evaluate the effect of L on the electric field strength. Fig. S7 demonstrates that, as L increases from 2 cm to 5 cm, the electric field strength decreases significantly. In Fig. 5b, the results for the maximum electric field strength with various distances are obtained by COMSOL calculation, where the maximum electric field strength decreases from 7.65×10^6 V/m to 5.4×10^6 V/m as L increases. In Fig. 5c, experimental results of the NAIs generation rate are shown when using the PMC-IV to power a
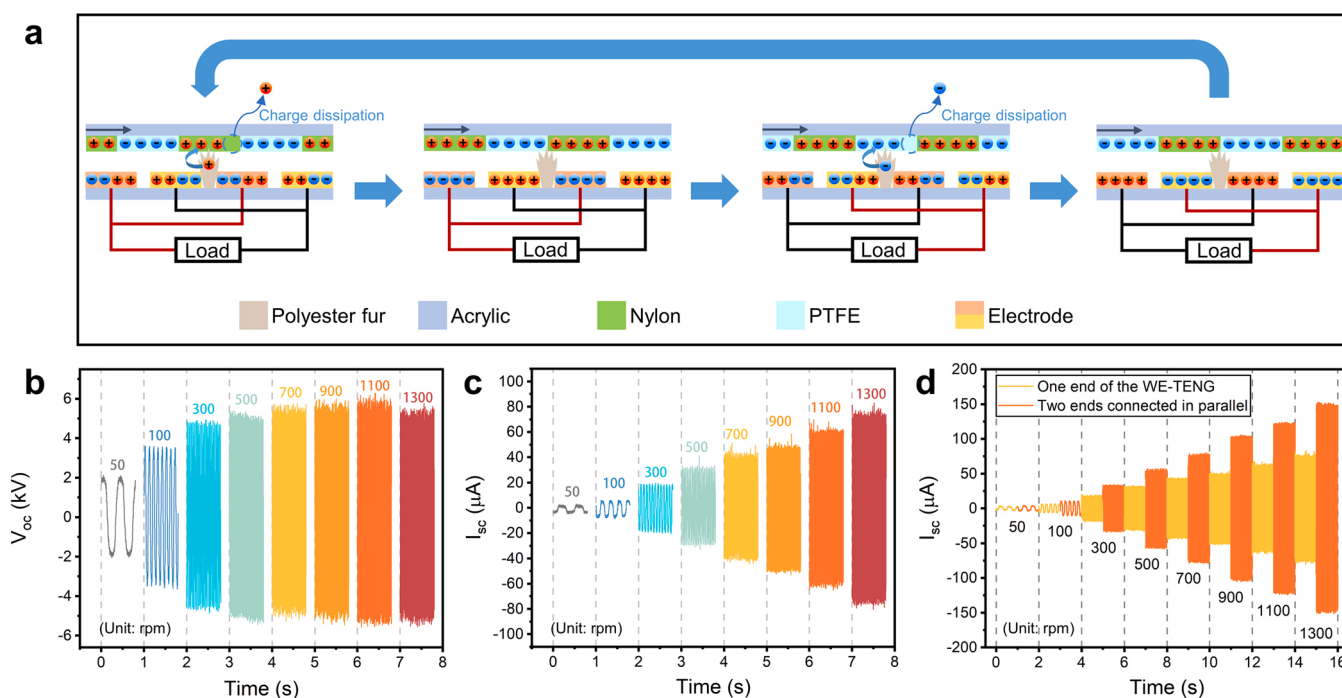

Fig. 3. Electrical output characteristics of the WE-TENG. (a) The working mechanism of the WE-TENG. (b) Open-circuit voltage and (c) short-circuit current at one end of the WE-TENG with a speed range of 50–1300 rpm. (d)The short-circuit current of both ends of the WE-TENG connected in parallel versus that of one end of the WE-TENG.
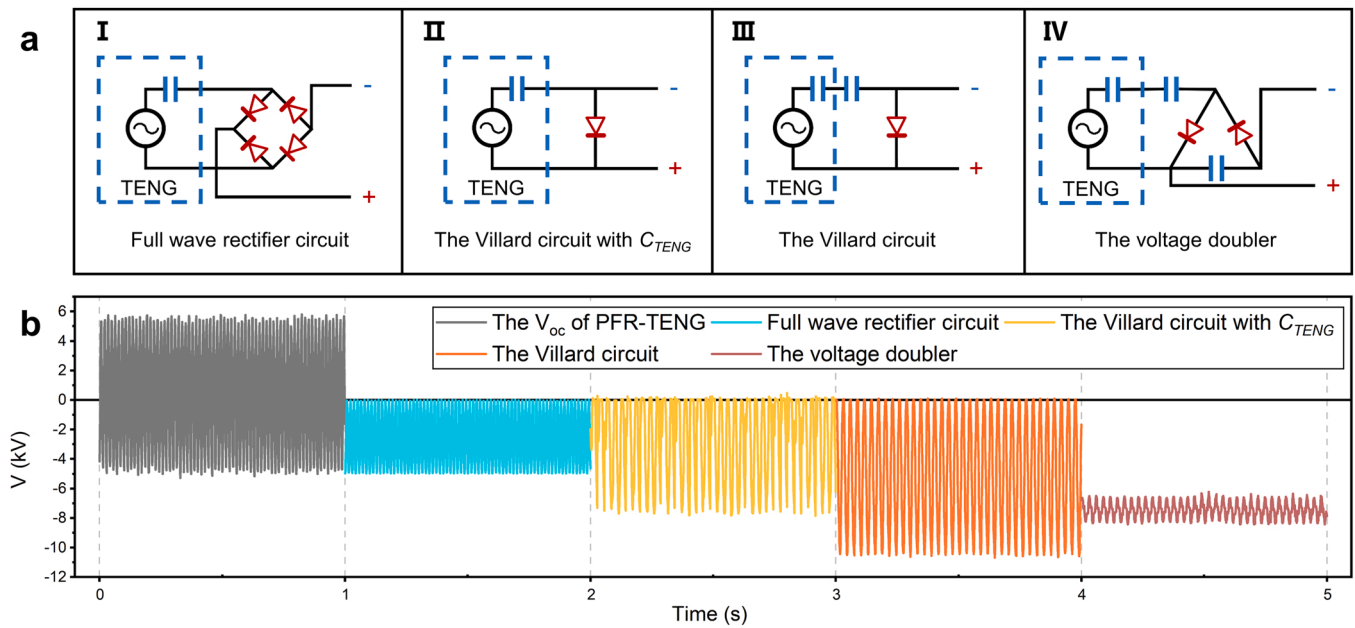
Fig. 4. The power management of the WE-TENG. (a) The circuit diagrams of four PMCs, including (PMC-I) the full wave rectifier circuit, (PMC-II) the Villard circuit with C_{TENG}, (PMC-III) the Villard circuit, and (PMC-IV) the voltage doubler. (b) The output voltage of four PMCs powered by the WE-TENG at a rotation speed of 700 rpm.

single carbon-fiber electrode. The experimental results are consistent with the simulation results, as L decreases, the generation rate of NAIs increases with the enhancement of the electric field strength.

According to Fig. 4b, the PMC-III has a pulsating DC output with the largest peak voltage while the output of the PMC-IV is more stable. Therefore, the experiments of these two PMCs driving the generation of NAIs with the three different electrodes are performed, and the results are shown in Fig. 5d & 5e. Obviously, the NAIs generation rate of the carbon-fiber electrode is higher than the other two electrodes, regardless of whether the PMC-III or the PMC-IV is used. Fig. 5f compares the generation rates of NAIs using the PMC-III and the PMC-IV at different n. As expected, the generation rate of NAIs is higher when using the latter because the root mean square (RMS) voltage of the former is not as high as that of the latter. In addition, the pulsating DC voltage cannot always be above the threshold voltage at which NAIs can be generated. Therefore, using the PMC-IV driving carbon-fiber electrodes to generate NAIs is an optimal choice.

To investigate the relationship between the generation rate of NAIs and the air purification performance, we carry out a series of experiments on air purification with the self-powered NAI generator. Each experiment is started after 60 s of releasing pollutants by lighting incense in an acrylic cylinder of 15 cm diameter and 30 cm height. The PM2.5 index of the air within the acrylic cylinder surpasses the measurement range of the instrument, with the maximum value being recorded at 999.

Fig. 5g visually shows the effect of air purification using a single carbon-fiber driven by the PMC-IV versus that without using the self-powered NAI generator. As the self-powered NAI generator is operating, NAIs are released through the copper mesh and into the air with forced convection, see the principle in Fig. 1c. It is proved that air purification by the self-powered NAI generator is feasible and effective. This is also demonstrated by the **supporting video 2**, where three types of electrodes are used to investigate the ability of air purification under forced convection by a fan. The rates of air purification of the self-powered NAI generator with the three electrodes coincide with the generation rates of NAIs shown in Fig. 5e. In particular, the most efficient air purification is achieved by using the carbon-fiber electrode, where the smoke has disappeared after operating for about 80 s. By

comparison, using the needle and tungsten alloy electrodes needs more time to achieve the same level of air purification.

Supplementary material related to this article can be found online at doi:10.1016/j.nanoen.2023.108459.

To enhance the air-purifying ability of the self-powered NAI generator, multiple carbon-fiber electrodes are used to generate NAIs simultaneously. Fig. 6 shows the experimental results. As expected, the generation rate of NAIs generally rises with increasing the number (N) of carbon-fiber electrodes (Fig. 6a). In particular, the rising rate is rapid for $N < 11$ and becomes slow at $N > 11$. Fig. S8 shows the rate of NAIs generation using 11 carbon-fiber electrodes at different n. It is obvious that the use of 21 carbon-fiber electrodes does improve compared to $N = 11$ but the effect is limited. Therefore, when $N > 11$, it is not cost-effective to increase the performance of the self-powered NAI generator.

To investigate the reasons for the variation in the NAIs generation rate, it is necessary to quantify the voltage and current at each electrode. Fig. S9 shows the equivalent circuit of the self-powered NAI generator when using multiple carbon-fiber electrodes. Here, the equivalent internal resistance of carbon-fiber electrodes generating NAIs is equivalent to a parallel connection. The theoretical output voltage of the PMC-IV (V_{output}) is given below [39,40]:

$$V_{output} = 2V_{input} - \Delta V \tag{2}$$

$$\Delta V = I_{output}/fC \tag{3}$$

where V_{input} is the peak voltage of the TENG, ΔV is the voltage loss, I_{output} is the output current, f is the frequency of the TENG, and C is the capacity of the capacitor used in the PMC-IV. When the self-powered NAI generator uses multiple electrodes, changes in load affect the output of the PMC-IV, and I_{output} obviously increases. From Eqs. (2) & (3), it can be seen that V_{output} decreases as I_{output} increases, implying that the voltage on each carbon-fiber electrode decreases when N is increased. Based on the results of Figure 6a and Eqs. (2) & (3), the theoretical V_{output} should be:

$$V_{output} \approx 1.1 \times 10^4 - 2.86 \times 10^6 I_{output} \tag{4}$$

However, the C_{TENG} is much smaller than the capacitance used in the PMC-IV, and the output waveform of the WE-TENG is not strictly
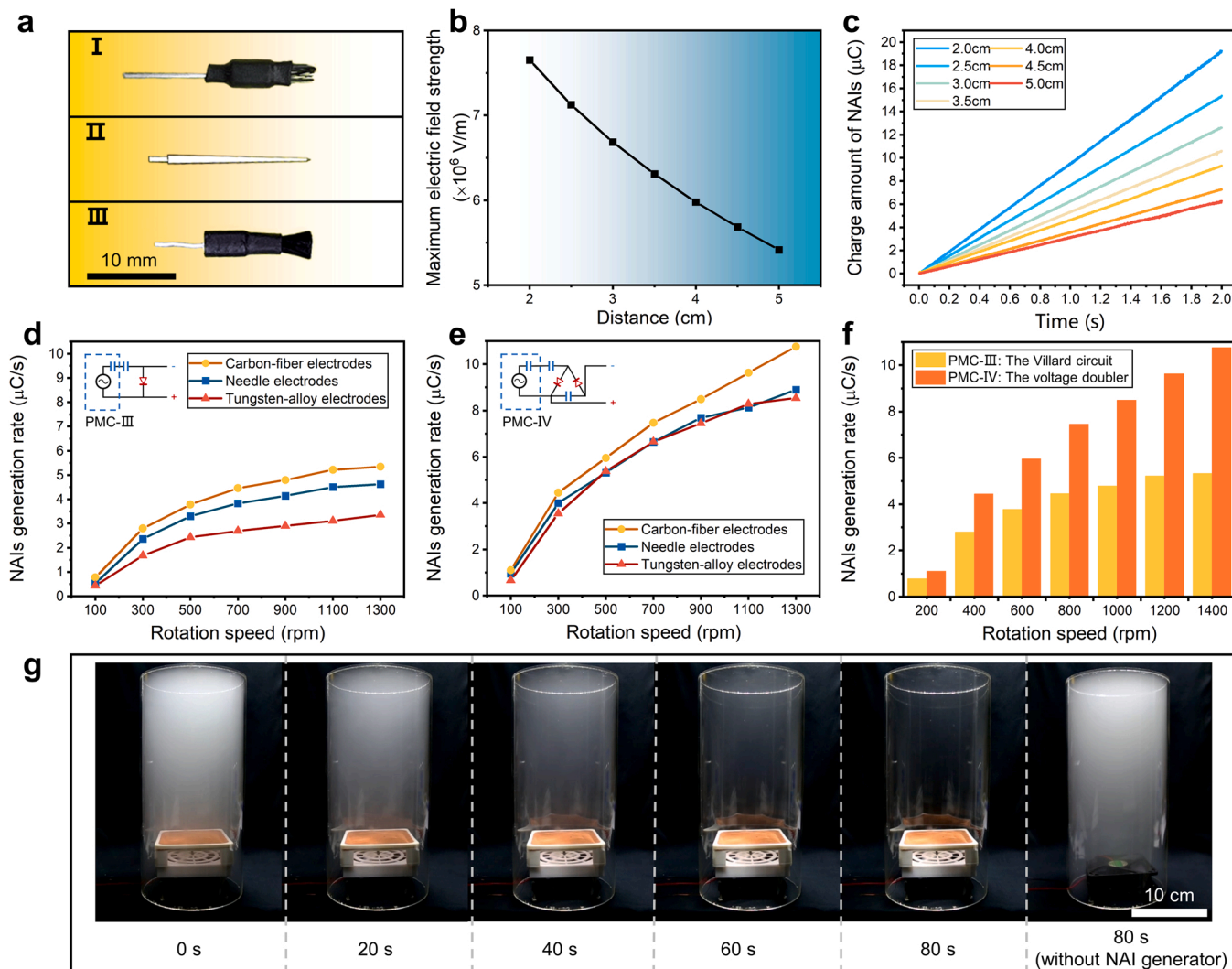
Fig. 5. Effect of different parameters on the performance of self-powered NAI generator to generate NAIs. (a) Photos of (I) the tungsten-alloy, (II) needle, and (III) carbon-fiber electrodes. (b) Simulation results of the maximum electric field strength at different distances (*L*) between the electrodes and the copper mesh. (c) Experimental results on the effect of *L* in generating the NAIs. Using (d) the PMC-III and (e) the PMC-IV to power three different electrodes to generate NAIs at different speeds of WE-TENG. (f) Comparison of the generation rate of NAIs when using the PMC-III and the PMC-IV. (g) Air purification using a single carbon fiber electrode powered by the WE-TENG with the PMC-IV.

sinusoidal, so the actual V_{output} should be smaller than the theoretical value. Therefore, the voltage on the electrodes cannot be calculated using Eq. (4). Thus, the current-voltage curve of the PMC-IV powered by WE-TENG needs to be obtained through experiment.

The actual V_{output} is obtained by measuring I_{output} of different resistive loads on PMC-IV and calculated by Ohm's law. The results are shown in Fig. 6b. When the resistance of the load is between 0.1 GΩ and 3 GΩ, the PMC-IV reaches the maximum output voltage, see Fig. 6c, I_{output} and V_{output} are related approximately linearly as follows :

$$V_{output} = 8.33 \times 10^3 - 2.84 \times 10^8 I_{output} \tag{5}$$

which shows that C_{TENG} greatly enhances the value of ΔV, but the overall trend is still consistent with Eqs. (2) & (3).

By bringing I_{output} of different N into the Eq. (5), the voltages on each carbon-fiber electrode are shown in Fig. 6d. As N increases, the voltage and the current on each electrode decreases. Theoretically, the voltage and current will be reduced with N increases, until the voltage on the electrode is below the threshold voltage for the generation of NAIs.

Last but not least, an experiment on air purification using the self-powered NAI generator with different numbers of carbon-fiber

electrodes is carried on. As shown in Fig. 6e, the air purification performance of the self-powered NAI generator with multiple carbon-fiber electrodes did improve significantly compared with a single carbon-fiber electrode. Further, there is a relatively small improvement in air purification capacity when using 21 or 11 carbon-fiber electrodes, which is consistent with Fig. 6a. In **supporting video 3**, the air purification performance of the self-powered NAI generator with different amounts of carbon-fiber electrodes is shown. The air in the acrylic without the self-powered NAI generator is also compared with using the self-powered NAI generator. The self-powered NAI generator exhibits excellent air purification capability, thus showing the potential that it can build a self-powered air purification system and implement practical applications.

Supplementary material related to this article can be found online at doi:10.1016/j.nanoen.2023.108459.

3. Conclusion

As well known, traditional in-pipe air purification equipment faces challenges due to its complex power supply and maintenance requirements. The present study has proposed a novel TENG-based NAI
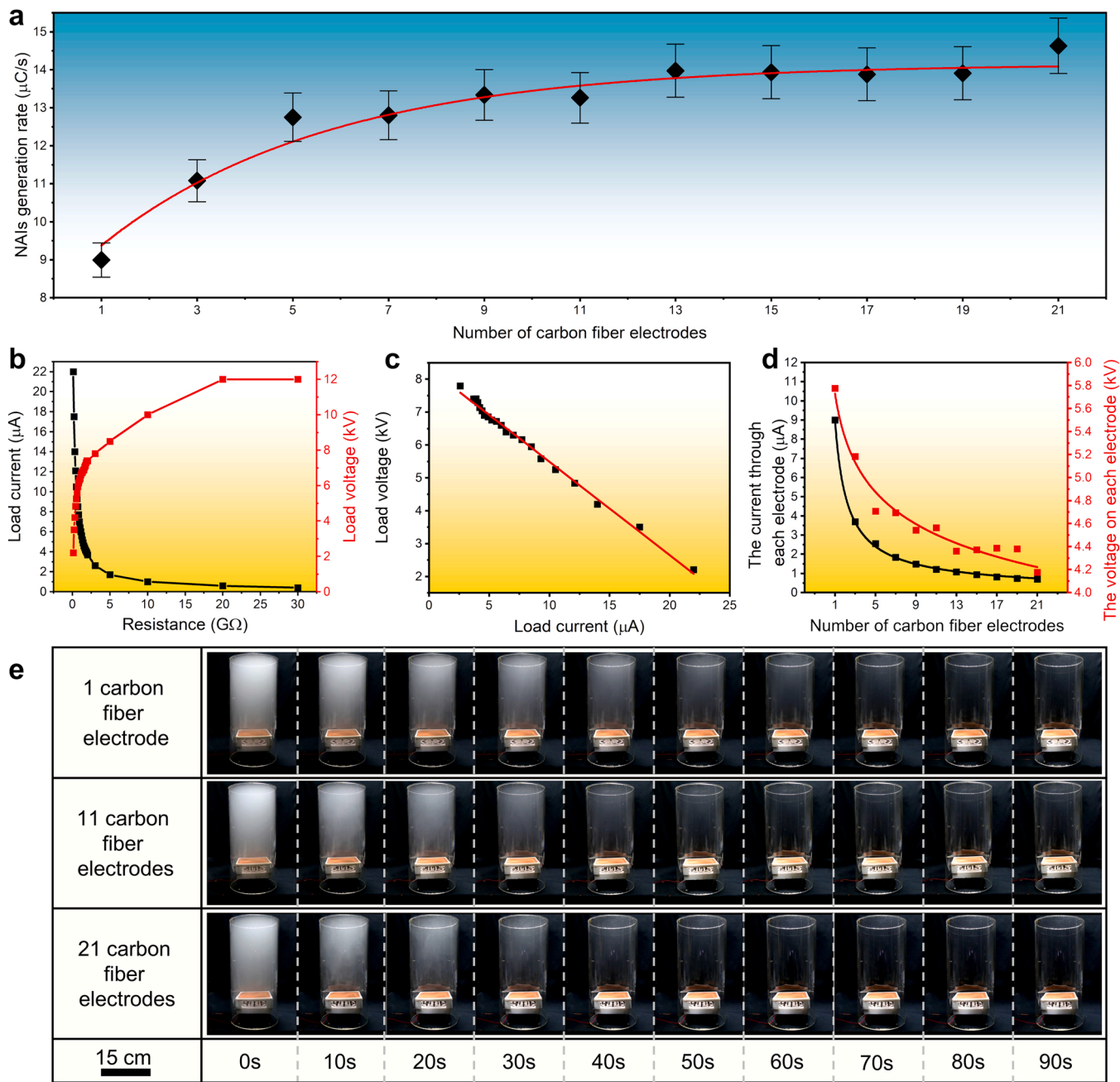
Fig. 6. Performances of the self-powered NAI generator operating with various numbers of carbon-fiber electrodes. (a) The generation rate of NAIs at 700 rpm. (b) The current and voltage at different loads on the PMC-IV. (c) The relationship between the output voltage and current of the PMC-IV. (d) The current and the voltage across each electrode when the PMC-IV drives different numbers of carbon-fiber electrodes. (e) Air purification performance of the self-powered NAI generator with different numbers of carbon-fiber electrodes.

generator that addresses these challenges. Compared to previous TENG-based air purification solutions, our work can be better adapted to the application scenario inside the air pipeline. As a specific example, the WE-TENG can start at low wind speeds and attains a rotational speed of up to 1300 rpm within the pipeline. The WE-TENG has a pressure drop of only 175 Pa at 1300 rpm, which ensures minimal impact on the pipeline. WE-TENG efficiently converts wind energy into continuous rotation, enabling the NAI generator to continuously generate NAIs compared to TENGs that collect vibration or reciprocating motion. The continuous power supply of the WE-TENG makes it possible for the PMC to adjust the voltage of the WE-TENG to a continuous and stable HV-DC, which allows the NAI generator to keep the voltage which can release a large amount of NAIs. In one second, the self-powered NAI generator can

generate NAIs of 23 μC. The electrical characteristics of different numbers of electrodes driven by the PMC have also been quantified, which provides a demonstration for other similar HV studies based on TENG. The NAIs released from self-powered NAI generators are verified to be effective in air purification, which provides a solid foundation for the practical application of TENG-based self-powered air purification systems.

4. Experimental section

4.1. Fabrication of the WE-TENG

The WE-TENG consists of two PFR-TENGs and two blades for wind

energy harvesting. The WE-TENG is 20 cm in diameter and 20 cm in length. 3D printing technology is used for production and the PLA-LW (ePLA-LW, Shenzhen Esun Industrial Co., Ltd.) is selected as the material for 3D printing. The cross-section of the air pipe where the WE-TENG is located is a square with a side length of 25 cm. The PFR-TENG is produced by 3D printing using PLA-LW material. Both the rotor and stator have a diameter of 20 cm and a thickness of 3 mm. Two rotors are joined to the blade and form the WE-TENG. The nylon and PTFE films are alternately adhered to the rotor using Kapton double-sided adhesive. The thicknesses of nylon and PTFE films are both 0.05 mm. Six pieces of copper foil are adhered to the stator, forming three pairs of electrodes. Two pieces of polyester fur with 5 mm wide and 9 cm long are fixed in the gap between the electrodes. All videos are shot by CANON EOS 5D Mark III.

4.2. Electrical measurements of the self-powered NAI generator

The short-circuit current of the WE-TENG is obtained by the Keithley 6514 electrometer (version Keithley 6514, impedance>200 TΩ, The Keithley. Inc., USA). The open-circuit voltage is measured by the Keithley DMM 6500 electrometer (The Keithley. Inc., USA) with a high-voltage probe (version HVP-40, 1/1000, The Pintech. Inc., China). The amount of NAIs generated by the self-powered NAI generator is obtained through the charge measurement function of the Keithley 6514, which directly measures the amount of charge passing through the carbon-fiber electrode.

4.3. Fabrication and measurements of circuit management

The PMCs are made with T77 diodes (withstanding voltage 20 kV) and capacitors with a capacity of 10 nF (withstanding voltage 20 kV) on the PCB. The output voltage is measured by the Keithley DMM 6500 system electrometer with a high-voltage probe (version HVP-40, 1/1000, The Pintech. Inc., China), which is equivalent to the output voltage of the circuit at 1GΩ load. The output voltage of the PMC connecting to different loads is obtained by using Keithley 6514 to measure the current and calculated by Ohm's Law.

CRediT authorship contribution statement

Fangming Li: Conceptualization, Methodology, Validation, Writing – original draft, Writing – review & editing, Visualization. **Cuiwen Deng**: Conceptualization, Validation, Formal analysis, Visualization. **Minzheng Sun**: Methodology, Investigation. **Xingfu Wan**: Validation, Investigation, Visualization. **Shuowen Sun**: Methodology, Investigation, Data curation. **Weipeng Xu**: Validation, Formal analysis, Investigation. **Taili Du**: Resources, Writing – review & editing, Project administration. **Yongjiu Zou**: Resources, Writing – review & editing. **Haichao Yuan**: Resources, Writing – review & editing. **Xinxiang Pan:** Conceptualization, Supervision. **Jianchun Mi**: Writing – original draft, Writing – review & editing, Supervision. **Minyi Xu**: Conceptualization, Resources, Supervision, Funding acquisition, Writing – review & editing.

Declaration of Competing Interest

The authors declare that they have no known competing financial interests or personal relationships that could have appeared to influence the work reported in this paper.

Data availability

Data will be made available on request.

Appendix A. Supporting information

Supplementary data associated with this article can be found in the online version at doi:10.1016/j.nanoen.2023.108459.

References

[1] G. Geng, Y. Zheng, Q. Zhang, T. Xue, H. Zhao, D. Tong, B. Zheng, M. Li, F. Liu, C. Hong, K. He, S.J. Davis, Drivers of PM2.5 air pollution deaths in China 2002–2017, Nat. Geosci. 14 (2021) 645–650, https://doi.org/10.1038/s41561-021-00792-3.

[2] J. Lelieveld, J.S. Evans, M. Fnais, D. Giannadaki, A. Pozzer, The contribution of outdoor air pollution sources to premature mortality on a global scale, Nature 525 (2015) 367–371, https://doi.org/10.1038/nature15371.

[3] T. Vandyck, K. Keramidas, A. Kitous, J.V. Spadaro, R. Van Dingenen, M. Holland, B. Saveyn, Air quality co-benefits for human health and agriculture counterbalance costs to meet Paris Agreement pledges, Nat. Commun. 9 (2018) 4939, https://doi.org/10.1038/s41467-018-06885-9.

[4] N. Bruce, R. Perez-Padilla, R. Albalak, Indoor air pollution in developing countries: a major environmental and public health challenge, Bull. World Health Organ 78 (2000) 1078–1092. <Go to ISI>://WOS:000089263900003.

[5] X. Lu, Z. O'Neill, Y. Li, F. Niu, A novel simulation-based framework for sensor error impact analysis in smart building systems: A case study for a demand-controlled ventilation system, Appl. Energy 263 (2020), 114638, https://doi.org/10.1016/j.apenergy.2020.114638.

[6] T.M.R. de, C. Curi, D. Conti, R. do, A. Vercellino, J.M. Massari, D.J. de Moura, Z. M. de Souza, R. Montanari, Positioning of sensors for control of ventilation systems in broiler houses: a case study, Sci. Agric. 74 (2017) 101–109, https://doi.org/10.1590/1678-992x-2015-0369.

[7] A. Singh, Y. Pandey, A. Kumar, M.K. Singh, A. Kumar, S.C. Mukhopadhyay, Ventilation Monitoring and Control System for High Rise Historical Buildings, IEEE Sens J. 17 (2017) 7533–7541, https://doi.org/10.1109/JSEN.2017.2756978.

[8] M. Hajikhani, F. Labeau, B.L. Agba, An autonomous wireless sensor network in a substation area using wireless transfer of energy, IEEE Access 6 (2018) 62352–62360, https://doi.org/10.1109/ACCESS.2018.2876265.

[9] C. Han, Maintenance of electrical equipment and wiring of new energy vehicles, J. Phys. Conf. Ser. 1550 (2020), 052028, https://doi.org/10.1088/1742-6596/1550/5/052028.

[10] C. Schantz, K. Gerhard, J. Donnal, J. Moon, B. Sievenpiper, S. Leeb, K. Thomas, Retrofittable Machine Condition and Structural Excitation Monitoring From the Terminal Box, IEEE Sens J. 16 (2016) 1224–1232, https://doi.org/10.1109/JSEN.2015.2498626.

[11] F.-R. Fan, Z.-Q. Tian, Z.L. Wang, Flexible triboelectric generator, Nano Energy 1 (2012) 328–334, https://doi.org/10.1016/j.nanoen.2012.01.004.

[12] C.-L. Li, W.-Z. Song, D.-J. Sun, M. Zhang, J. Zhang, Y.-Q. Chen, S. Ramakrishna, Y.-Z. Long, A self-priming air filtration system based on triboelectric nanogenerator for active air purification, Chem. Eng. J. 452 (2023), 139428, https://doi.org/10.1016/j.cej.2022.139428.

[13] Y. Feng, L. Ling, J. Nie, K. Han, X. Chen, Z. Bian, H. Li, Z.L. Wang, Self-powered electrostatic filter with enhanced photocatalytic degradation of formaldehyde based on built-in triboelectric nanogenerators, ACS Nano 11 (2017) 12411–12418, https://doi.org/10.1021/acsnano.7b06451.

[14] H. Guo, J. Chen, L. Wang, A.C. Wang, Y. Li, C. An, J.-H. He, C. Hu, V.K.S. Hsiao, Z. L. Wang, A highly efficient triboelectric negative air ion generator, Nat. Sustain 4 (2020) 147–153, https://doi.org/10.1038/s41893-020-00628-9.

[15] G.Q. Gu, C.B. Han, C.X. Lu, C. He, T. Jiang, Z.L. Gao, C.J. Li, Z.L. Wang, Triboelectric nanogenerator enhanced nanofiber air filters for efficient particulate matter removal, ACS Nano 11 (2017) 6211–6217, https://doi.org/10.1021/acsnano.7b02321.

[16] S. Chen, C. Gao, W. Tang, H. Zhu, Y. Han, Q. Jiang, T. Li, X. Cao, Z. Wang, Self-powered cleaning of air pollution by wind driven triboelectric nanogenerator, Nano Energy 14 (2015) 217–225, https://doi.org/10.1016/j.nanoen.2014.12.013.

[17] Z.-Y. Huo, Y.-J. Kim, I.-Y. Suh, D.-M. Lee, J.H. Lee, Y. Du, S. Wang, H.-J. Yoon, S.-W. Kim, Triboelectrification induced self-powered microbial disinfection using nanowire-enhanced localized electric field, Nat. Commun. 12 (2021) 3693, https://doi.org/10.1038/s41467-021-24028-5.

[18] C. Li, H. Guo, Z. Wu, P. Wang, D. Zhang, Y. Sun, Self-Healable Triboelectric Nanogenerators: Marriage between Self-Healing Polymer Chemistry and Triboelectric Devices, Adv. Funct. Mater. 33 (2023) 2208372, https://doi.org/10.1002/adfm.202208372.

[19] C. Wang, H. Guo, P. Wang, J. Li, Y. Sun, D. Zhang, An Advanced Strategy to Enhance TENG Output: Reducing Triboelectric Charge Decay, Adv. Mater. N./a (2023) 2209895, https://doi.org/10.1002/adma.202209895.

[20] J. Chen, X. Wei, B. Wang, R. Li, Y. Sun, Y. Peng, Z. Wu, P. Wang, Z.L. Wang, Design Optimization of Soft-Contact Freestanding Rotary Triboelectric Nanogenerator for High-Output Performance, Adv. Energy Mater. 11 (2021) 2102106, https://doi.org/10.1002/aenm.202102106.

[21] L. Long, W. Liu, Z. Wang, W. He, G. Li, Q. Tang, H. Guo, X. Pu, Y. Liu, C. Hu, High performance floating self-excited sliding triboelectric nanogenerator for micro mechanical energy harvesting, Nat. Commun. 12 (2021) 4689, https://doi.org/10.1038/s41467-021-25047-y.

[22] W. Deng, Y. Zhou, X. Zhao, S. Zhang, Y. Zou, J. Xu, M.-H. Yeh, H. Guo, J. Chen, Ternary electrification layered architecture for high-performance triboelectric nanogenerators, ACS Nano 14 (2020) 9050–9058, https://doi.org/10.1021/acsnano.0c04113.

[23] Y. Bai, L. Xu, S. Lin, J. Luo, H. Qin, K. Han, Z.L. Wang, Charge pumping strategy for rotation and sliding type triboelectric nanogenerators, Adv. Energy Mater. 10 (2020) 2000605, https://doi.org/10.1002/aenm.202000605.

[24] X. Li, J. Luo, K. Han, X. Shi, Z. Ren, Y. Xi, Y. Ying, J. Ping, Z.L. Wang, Stimulation of ambient energy generated electric field on crop plant growth, Nat. Food 3 (2022) 133–142, https://doi.org/10.1038/s43016-021-00449-9.

[25] F. Zheng, Y. Zhou, S. Hu, R. Li, Z.L. Wang, Z. Wu, A hybridized triboelectric-electromagnetic nanogenerator as a power supply of monitoring sensors for the ventilation system, Adv. Energy Mater. 12 (2022) 2201966, https://doi.org/10.1002/aenm.202201966.

[26] H. Dang, Y. Wang, S. Zhang, Q. Gao, X. Li, L. Wan, Z.L. Wang, T. Cheng, Triboelectric-electromagnetic hybrid generator with the inertia-driven conversion mechanism for wind energy harvesting and scale warning, Mater. Today Energy 29 (2022), 101136, https://doi.org/10.1016/j.mtener.2022.101136.

[27] X. Li, Q. Gao, Y. Cao, Y. Yang, S. Liu, Z.L. Wang, T. Cheng, Optimization strategy of wind energy harvesting via triboelectric-electromagnetic flexible cooperation, Appl. Energy 307 (2022), 118311, https://doi.org/10.1016/j.apenergy.2021.118311.

[28] D. Liu, C. Li, P. Chen, X. Zhao, W. Tang, Z.L. Wang, Sustainable long-term and wide-area environment monitoring network based on distributed self-powered wireless sensing nodes, Adv. Energy Mater. 13 (2023) 2202691, https://doi.org/10.1002/aenm.202202691.

[29] X. Fan, J. He, J. Mu, J. Qian, N. Zhang, C. Yang, X. Hou, W. Geng, X. Wang, X. Chou, Triboelectric-electromagnetic hybrid nanogenerator driven by wind for self-powered wireless transmission in Internet of Things and self-powered wind speed sensor, Nano Energy 68 (2020), 104319, https://doi.org/10.1016/j.nanoen.2019.104319.

[30] Y. Gui, Y. Wang, S. He, J. Yang, Self-powered smart agriculture real-time sensing device based on hybrid wind energy harvesting triboelectric-electromagnetic nanogenerator, Energy Convers. Manag 269 (2022), 116098, https://doi.org/10.1016/j.enconman.2022.116098.

[31] H.-X. Zou, L.-C. Zhao, Q. Wang, Q.-H. Gao, G. Yan, K.-X. Wei, W.-M. Zhang, A self-regulation strategy for triboelectric nanogenerator and self-powered wind-speed sensor, Nano Energy 95 (2022), 106990, https://doi.org/10.1016/j.nanoen.2022.106990.

[32] F. Li, X. Wan, J. Hong, X. Guo, M. Sun, H. Lv, H. Wang, J. Mi, J. Cheng, X. Pan, M. Xu, Z.L. Wang, A self-powered and efficient triboelectric dehydrator for separating water-in-oil emulsions with ultrahigh moisture content, Adv. Mater. Technol. 7 (2022) 2200198, https://doi.org/10.1002/admt.202200198.

[33] J. Tan, P. Tian, M. Sun, H. Wang, N. Sun, G. Chen, Y. Song, D. Jiang, H. Jiang, M. Xu, A transparent electrowetting-on-dielectric device driven by triboelectric nanogenerator for extremely fast anti-fogging, Nano Energy 92 (2022), 106697, https://doi.org/10.1016/j.nanoen.2021.106697.

[34] K. Han, J. Luo, J. Chen, Y. Liu, J. Li, Z.L. Wang, W. Mai, Plastic film based lightweight thruster driven by triboelectric nanogenerator for multi-purpose propulsion applications, Nano Energy 101 (2022), 107558, https://doi.org/10.1016/j.nanoen.2022.107558.

[35] H.-F. Lin, J.-M. Lin, Generation and determination of negative air ions, J. Anal. Test. 1 (2017) 6, https://doi.org/10.1007/s41664-017-0007-7.

[36] A. Hartmann, M. Kriegel, The influence of air ions on the particle concentration in indoor environments – A systematic literature review, Results Eng. 15 (2022), 100528, https://doi.org/10.1016/j.rineng.2022.100528.

[37] S.Y. Jiang, A. Ma, S. Ramachandran, Negative air ions and their effects on human health and air quality improvement, Int J. Mol. Sci. 19 (2018), https://doi.org/10.3390/ijms19102966.

[38] Z.L. Wang, On Maxwell's displacement current for energy and sensors: the origin of nanogenerators, Mater. Today 20 (2017) 74–82, https://doi.org/10.1016/j.mattod.2016.12.001.

[39] J.S. Brugler, Theoretical performance of voltage multiplier circuits, IEEE J. Solid-State Circuits 6 (1971) 132–135.

[40] S.H. Park, L. Katzir, D. Shmilovitz, Reduction of voltage drop and ripple in voltage multipliers, in: 2015 17th European Conference on Power Electronics and Applications (EPE'15 ECCE-Europe), IEEE, 2015: pp. 1–7. https://doi.org/10.1109/EPE.2015.7309074.

Fangming Li is currently pursuing his Ph.D. degree at Dalian Maritime University, China. His research mainly focuses on the performance improvement of triboelectric nanogenerators and high-voltage applications based on triboelectric nanogenerators.

Cuiwen Deng received her B. Eng from Guangzhou University in China in 2019. Currently, she is a postgraduate student at Marine Engineering College, Dalian Maritime University. Her current research work focuses on wind energy harvesting and self-powered air purification based on triboelectric nanogenerators.

Minzheng Sun received his B.S. from Dalian Maritime University in China in 2021. Currently, he is a postgraduate student at Marine Engineering College, Dalian Maritime University. His current research work focuses on wind energy harvesting and self-powered sensing based on triboelectric nanogenerators.

Xingfu Wan received his B.S. degree from Dalian Maritime University in 2018 and is currently pursuing his M.S. degree at Dalian Maritime University. His main research interests include the study of high voltage characteristics of triboelectric nanogenerators and applications in electrohydrodynamics.

Shuowen Sun is currently pursuing a master's degree at Dalian Maritime University, China. His current research interests include flow-induced vibration, wind energy harvesting, ocean current energy harvesting, and triboelectric nanogenerator.

Weipeng Xu is currently in his third year of undergraduate studies at the College of Marine Engineering, Dalian Maritime University. His current research work focuses on self-powered sensing based on triboelectric nanogenerators.

Xinxiang Pan received his B.E and Ph.D. degrees from Marine Engineering College, Dalian Maritime University, China, in 1987 and 1999. He now is President of Guangdong Ocean University. His research interests include smart and green ship, ocean engineering, energy saving and emission reduction, ship safety and pollution control, microfluidic chip, nano energy and self-powered systems.

Taili Du has been with Dalian Maritime University where he is currently an Associate Professor since 2010. He received his B. S. and M.S. from Dalian Maritime University in China in 2008 and 2010, and he is a doctoral candidate at Marine Engineering College, Dalian Maritime University. His current research work focuses on vibration energy harvesting and self-powered vibration sensor based on Triboelectric Nanogenerator.

Prof. Jianchun Mi received his Ph.D. degrees from Newcastle University in 1995. He was a national researcher and director researcher of Adelaide University in Australia from 1995 to 2006. He joined Peking University in 2006, and now he is a full professor in the College of Engineering. His research interests include turbulence, combustion and renewable energy.

Yongjiu Zou is an assistant professor at the College of Marine Engineering, Dalian Maritime University. He received his B.S. and M.S. in marine engineering both from Dalian Maritime University in 2012 and 2014, respectively. He spent a year as a visiting scholar at University of California, Los Angeles under the supervision of Prof. Jun Chen in 2020. His research focuses on triboelectric nanogeneraters for energy harvesting and self-powered sensing.

Minyi Xu received his Ph.D. degree from Peking University in 2012. During 2016–2017, he joined Professor Zhong Lin Wang's group at Georgia Institute of Technology. Now he is a Professor in the Marine Engineering College, Dalian Maritime University. His current research is mainly focused on the areas of blue energy, self-powered systems, triboelectric nanogenerators and their practical applications in smart ship and ocean.

Haichao Yuan received his Master's degree in Dalian Maritime University in 2014, he is now working in Dalian Maritime University. He is currently pursuing his doctor degree in Dalian Maritime University, China. His current research interests include energy harvesters, self-powered systems, triboelectric nanogenerators.